Supporting material for: Control of sarcoplasmic reticulum Ca^{2+} release by stochastic RyR gating within a 3D model of the cardiac dyad and importance of induction decay for CICR termination. Cannell, M.B., Kong, C.H.T., Imtiaz, M.S., Laver, D.R.

Supporting Methods

SR vesicle preparation

Liquid nitrogen-frozen hearts from rat and sheep were homogenized in buffer containing (in mM): 10 imidazole, 0.5 dithiothreitol, 3 sodium azide, 290 sucrose, 1 benzamidine, 0.5 PMSF, 20 NaF (for rat only) with 1 μg/ml leupeptin and 1μg/ml pepstatin A, pH 6.9 (homogenization buffer). Homogenization was carried in 3x15 s bursts with a rotor-stator homogenizer (HD Scientific) followed by 10 manual strokes of a loose glass/glass Dounce homogenizer. The homogenate was then centrifuged at 7000 rpm for 20 min in Beckman Optima L-100XP Ultracentrifuge. The resulting supernatant was centrifuged at 50000 rpm for 30 min. The pellet from this step was re-homogenized with a tight manual glass/glass Dounce homogenizer in homogenization buffer also containing 0.65 M KCl (storage buffer, pH 6.7), incubated for 30 min and then centrifuged at 7000 rpm for 15 min. The supernatant was centrifuged at 50000 rpm for 1 hr, and the resulting pellet was resuspended in storage buffer, snap frozen in liquid nitrogen and stored at -80°C. The NaF present in our buffers was to prevent ongoing activity of phosphatases (PP1 and PP2A) during SR vesicle preparation. The whole procedure was carried out at 4 °C.

Solution preparation for single channel recordings

All solutions were made with MilliQ water and were pH buffered with 10 mM TES (*N*-tris [hydroxymethyl] methyl-2-aminoethanesulfonic acid; ICN Biomedicals) and adjusted to pH 7.4 by CsOH (ICN Biomedicals), using a TPS digital pH meter. Free [Ca^{2+}] (1-500 μM was buffered using 1 mM BAPTA plus 1 mM dibromo BAPTA. A Ca^{2+} electrode (Radiometer) was used to determine the purity of Ca^{2+} buffers, Ca^{2+} stock solutions and free [Ca^{2+}] in the experimental solutions against a 100 mM $CaCl_2$ standard (Fluka). The concentration of the Mg^{2+} stock solutions was calibrated against a 100 mM $MgCl_2$ standard (Fluka) using Mg-induced pH changes induced in EDTA containing solutions. The concentration of ATP was calibrated by measuring ATP chelation of Ca^{2+} standard solutions with a Ca^{2+} electrode. Free [Mg^{2+}] in the presence of ATP (sodium salt from Sigma Chemicals) was determined using estimates of ATP purity and effective Mg^{2+} binding constants as determined previously under our experimental conditions (1).

Computational model gridding

Ca^{2+} diffusion and binding to Ca^{2+} indicators (fluo-3 and fluo-5N), in and around the dyad, were calculated using Matlab (Mathworks, Inc., Natick, MA, USA) on a MacBook Pro computer with an i7 microprocessor and 8 Gb memory. The simulations required the solution of a system of ordinary

differential equations that were solved using a cylindrical coordinate system with a Matlab stiff ODE solver (ode15s). The cytoplasmic volume was divided into 18 slices along the axis of the tubule (z), 13 radial rings (r) and 16 segments around the axis (θ), amounting to 3744 volume elements. The j-SR volume was divided into ~192 volume elements (depending on j-SR dimensions with r=1) and the n-SR was divided into 280 elements (z=5, θ=7, r=8). Reflecting boundaries of the model were located at ±2μm along the t-tubule and at a radius of 2μm. The connection from the j-SR to n-SR is uncertain, from Brochet *et al.* (2) and Knollmann *et al.* (3), we estimate the equivalent diameter of the n-SR to j-SR tubules to be 31 nm, but without detailed tomographic data this is uncertain. Pragmatically, with the geometry used, the model reproduces the time course of restitution well so our geometry estimate appears reasonable.

Model RyR gating

The RyRs gating is simulated using a two state (open and closed) stochastic model where the opening and closing rates depend primarily on the local [Ca^{2+}] in the dyad cleft. In the model, the RyR gating rates have no explicit dependence on inactivation processes or allosteric interactions between RyRs. The rates of RyR opening and their dependence on [Ca^{2+}] was determined from single channel recording of rat and cardiac RyRs in the presence of various luminal [Ca^{2+}] (0.1 and 1 mM) and cytoplasmic [Ca^{2+}] (1-500 μM) in the presence of 1 mM free Mg^{2+} in the cytoplasm. The experimental transition rates for RyR opening and closing were calculated from the reciprocal of the mean closed and open times, respectively. In the model, the experimental transition rates were represented by the following equations for rat RyRs:

$$maximum\left\{k_{open} = 3.17 \times 10^5 [Ca^{2+}]_{cyto}^{2.8} \;;\quad k_{open} = 700\right\}$$

$$minimum\left\{k_{close} = 250[Ca^{2+}]_{cyto}^{-0.5} \;;\quad k_{close} = 900\right\}$$

For sheep RyRs, the opening and closing rates were given by:

$$maximum\left\{k_{open} = 4.57 \times 10^5 \,[Ca^{2+}]_{cyto}^{2.12} \;;\quad k_{open} = 800\right\}$$

$$k_{close} = 245\,[Ca^{2+}]_{cyto}^{-0.27}$$

The fit of these equations to experimental data is shown in Figure S1. Note that these equations are not designed to capture behaviour at resting [Ca^{2+}] with a fully loaded SR. We used a Monte-Carlo method to simulate the stochastic transitions of each RyR. While solving the ODE for ion diffusion, the integration process was allowed to progress beyond the anticipated time of next RyR transition, and using the solution to that point the RyR gating was modelled. This allowed the time dependent changes in the dyad to influence the Monte Carlo solution. If a RyR changed state, the model solution at that time was then taken as a new starting conditions (incorporating the new J_{RyR}) for the ODE

integrator, and the process repeated for as long as desired. If no RyR transition occurred the integration was continued for another period with its exit condition preserved (thereby avoiding the need for Jacobian re-evaluation). This approach allowed the solution of this very stiff problem to be advanced with reasonable efficiency as time steps could increase rapidly as transient terms in the solution decayed.

Model Ca^{2+} buffering by lipids

The presence in the membrane of negatively charged lipids such as phosphatidylserine (PS) and zwiterionic phosphatidylcholine (PC) gives rise to a negative net charge on the lipid bilayer, a negative electrostatic potential and provides binding sites for cations such as Ca^{2+} and K^+. In the model, these affects are treated using simplifying approximations as described for our previous model for Ca^{2+} diffusion and buffering in the dyad cleft (4) .

In our model of the t-tubule, the net electrostatic potential of the membrane surface is -55 mV, which remains constant throughout the spark simulations. The electrostatic potential falls off exponentially with a radial space constant of 1nm (the Debye length under physiological ionic conditions). The binding and unbinding rates for Ca^{2+} and K^+ to PS and PC were obtained from McLaughlin *et al.* (5) and these were used to calculate effective binding rates for Ca^{2+} in the presence of physiological [K^+] (145 mM) using the formula:

$$k_{on}^{eff} = k_{on} / \left(1 + \left(K_D^{K^+}[K^+]\right)\right)$$

where $K_D^{K^+}$ is the dissociation constant for K^+. We found that the total binding of Ca^{2+} to PC was 10^5 times lower than that for PS. Therefore, we did not include the effects of Ca^{2+} buffering by PC in the model.

Structural element	Value	Ref.
Computational radial boundary	2 μm	
Computational boundary along tubule axis	±2 μm	
RyR nearest neighbour separation	31 nm	(6, 7)
Radius of t-tubule	125 nm	(8)
Dyad cleft, separation between j-SR and t-tubule	15 nm	(9)
Thickness of j-SR	26 nm	(10)
Dyad length along t-tubule axis	360 nm	(11, 12)
Dyad circumference relative to t-tubule circumference	0.6	
Diameter of connecting tubule between j-SR and n-SR	31 nm	
Volume fraction of n-SR	0.035	(13)

Supporting Material Table S1: Model structural parameters

Species	Location	Concentration μM	Diffusion coefficient 10^{-10} m^2/s	k_{on} $(\mu Ms)^{-1}$	k_{off} s^{-1}
Ca^{2+}	cyto, cleft [a]	0.1	3.5	-	-
ATP	cyto, cleft [a]	5000	1.5	13.7 [b]	30000
Calmodulin	cyto, cleft [a]	36	0.45	100	31
fluo-4	cyto, cleft [a]	100	0.33	48.8	43.9
TroponinC	cyto	70	0	125	250
Ca^{2+}	j-SR	1000	3.5	-	-
fluo-5N	j-SR	100	0.33	48.8	19520
Calsequestrin [c]	j-SR	30000	0	39	78000
Ca^{2+}	n-SR	1000	0.6 [d]	-	-
fluo-5N	n-SR	100	0.01 [d]	48.8 [e]	19520 [e]
Calsequestrin	n-SR	6000	0	39	78000
SR lipids	cleft	47	0	125	250
PS	t-tubule	1.4 x 10^{6} [f]	0	30 [e]	2.5 x10^{6} [g]

Supporting Material Table S2: Diffusion and Buffering Coefficients. Values of concentrations, diffusion coefficients and Ca^{2+} buffering constants of various species included in the Ca^{2+} spark simulations. Unless otherwise stated, values were same as that used in our previous model for Ca^{2+} diffusion and buffering (4).

[a] Diffusion constants for the bulk cytoplasm are shown in the table. Diffusion constants in the cleft are 40% of those shown to allow for tortuosity in the diffusion paths due to the presence of large macromolecular complexes in the cleft (4).

[b] Effective on rate allowing for 14% free ATP at pH 7.2.

[c] Calsequestrin concentration estimated from Murphy *et al.* (14). Value of k_{on} was based on diffusion limited binding and k_{off} from Ikemoto *et al.* (15).

[d] Diffusion coefficients in the n-SR obtained from Wu *et al.* (16).

[e] Buffering Constants obtained Shannon *et al.* (17).

[f] Value derived from lipid mole fraction, lipid cross sectional area in membrane and the thickness of the lipid head group region in the bilayer.

[g] Value obtained from McLaughlin *et al.* (5).

Parameter	Value
Debye Length	1 nm
Electrostatic potential on t-tubule	-55 mV
PS mole fraction in t-tubule	0.3
RyR current (j-SR, 1mM Ca^{2+}; cyto 100nM Ca^{2+})	0.6 pA
DHPR current	0.2 pA
SERCa- maximum transport rate, $K_{sr,max}$	0.2 mM/s
SERCa- Binding constant for [Ca^{2+}] in SR, K_{SERCA}	5000 mM^{-1}

Supporting Material Table S3: Miscellaneous additional base model parameters

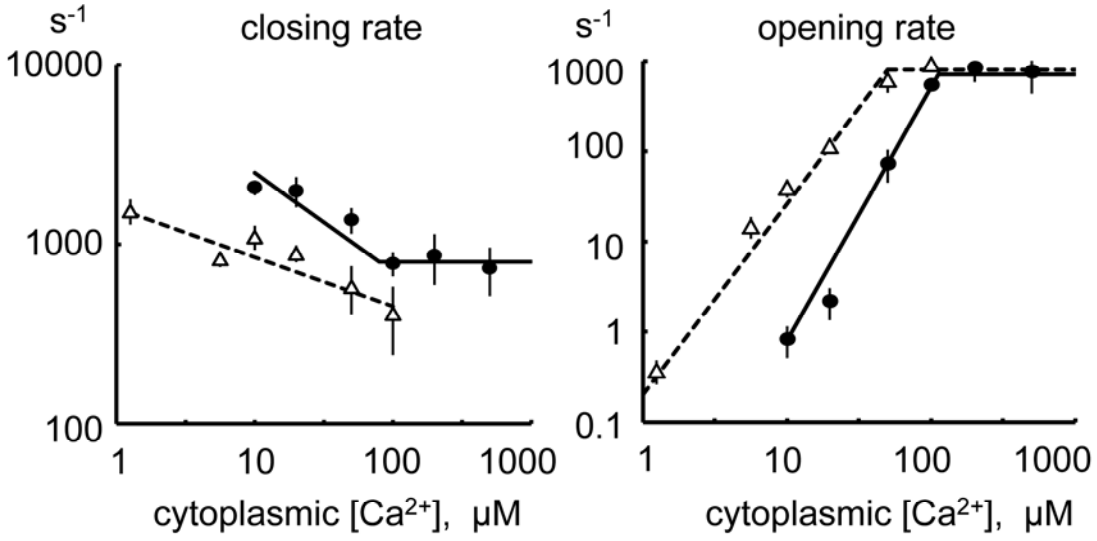

Supporting Figure S1 Comparison of model equations to gating data. Panels show closing (left) and opening rates (right) for sheep (open triangles) and rat (closed circles) RyRs. The rat data is replotted from (23).

Supporting References

1. Laver, D.R., E.R. O'Neill, and G.D. Lamb. 2004. Luminal Ca2+-regulated Mg2+ inhibition of skeletal RyRs reconstituted as isolated channels or coupled clusters. J. Gen. Physiol. 124: 741–758.

2. Brochet, D., D. Yang, A. Di Maio, W. Lederer, C. Franzini-Armstrong, et al. 2005. Ca2+ blinks: Rapid nanoscopic store calcium signaling. Proc. Natl. Acad. Sci. U.S.A. 102: 3099–3104.

3. Knollmann, B.C., N. Chopra, T. Hlaing, B. Akin, T. Yang, et al. 2006. Casq2 deletion causes sarcoplasmic reticulum volume increase, premature Ca2+ release, and catecholaminergic polymorphic ventricular tachycardia. J. Clin. Invest. 116: 2510–2520.

4. Soeller, C., and M.B. Cannell. 1997. Numerical simulation of local calcium movements during L-type calcium channel gating in the cardiac diad. Biophys. J. 73: 97–111.

5. McLaughlin, S., N. Mulrine, T. Gresalfi, G. Vaio, and A. McLaughlin. 1981. Adsorption of divalent cations to bilayer membranes containing phosphatidylserine. J. Gen. Physiol. 77: 445–473.

6. Protasi, F., C. Franzini-Armstrong, and B.E. Flucher. 1997. Coordinated incorporation of skeletal muscle dihydropyridine receptors and ryanodine receptors in peripheral couplings of BC3H1 cells. J. Cell Biol. 137: 859–870.

7. Saito, A., M. Inui, M. Radermacher, J. Frank, and S. Fleischer. 1988. Ultrastructure of the calcium release channel of sarcoplasmic reticulum. J. Cell Biol. 107: 211–219.

8. Soeller, C., and M.B. Cannell. 1999. Examination of the transverse tubular system in living cardiac rat myocytes by 2-photon microscopy and digital image-processing techniques. Circ. Res. 84: 266–275.

9. Fawcett, D.W., and N.S. McNutt. 1969. Ultrastructure of Cat Myocardium .I. Ventricular Papillary Muscle. J. Cell Biol. 42: 1–45.

10. Rizzi, N., N. Liu, C. Napolitano, A. Nori, F. Turcato, et al. 2008. Unexpected Structural and Functional Consequences of the R33Q Homozygous Mutation in Cardiac Calsequestrin: A Complex Arrhythmogenic Cascade in a Knock In Mouse Model. Circ. Res. 103: 298–306.

11. Franzini-Armstrong, C., F. Protasi, and V. Ramesh. 1999. Shape, size, and distribution of Ca(2+) release units and couplons in skeletal and cardiac muscles. Biophys. J. 77: 1528–1539.

12. Forbes, M.S., and N. Sperelakis. 1982. Bridging junctional processes in couplings of skeletal, cardiac, and smooth muscle. Muscle Nerve. 5: 674–681.

13. Bers, D.M. 2001. Excitation-Contraction Coupling and Cardiac Contractile Force. Kluwer Academic Pub.

14. Murphy, R.M., J.P. Mollica, N.A. Beard, B.C. Knollmann, and G.D. Lamb. 2011. Quantification of calsequestrin 2 (CSQ2) in sheep cardiac muscle and Ca2+-binding protein changes in CSQ2 knockout mice. Am. J. Physiol. Heart Circ. Physiol. 300: H595–H604.

15. Ikemoto, N., B. Nagy, G.M. Bhatnagar, and J. Gergely. 1974. Studies on a metal-binding protein of the sarcoplasmic reticulum. J. Biol. Chem. 249: 2357–2365.

16. Wu, X., and D.M. Bers. 2006. Sarcoplasmic reticulum and nuclear envelope are one highly interconnected Ca2+ store throughout cardiac myocyte. Circ. Res. 99: 283–291.

17. Shannon, T.R., T. Guo, and D.M. Bers. 2003. Ca2+ scraps: local depletions of free [Ca2+] in cardiac sarcoplasmic reticulum during contractions leave substantial Ca2+ reserve. Circ. Res. 93: 40–45.